The 18th Scandinavian International Conference on Fluid Power, SICFP'23, May 30- June 1, 2023, Tampere, Finland

State Estimation for a portal advancing mechanism by measuring the pressure in hydraulic actuators

Sebastian Beiser*, Lukas Michiels , and Marcus Geimer

Institute of Mobile Machines (Mobima)
Karlsruhe Institute of Technology (KIT)
Karlsruhe, Germany
E-mail: sebastian.beiser@kit.edu, lukas.michiels@kit.edu, marcus.geimer@kit.edu

Abstract

Leg-driven machines require complex control systems to ensure stability and safety. Instead of measuring the complete system state, state estimation and prediction can be used to observe the system state in hydraulically actuated systems to replace expensive sensors. In this paper, we consider the portal advancing mechanism, a legged locomotive mechanism. The overall machine consists of two bases with three hydraulically actuated legs each and a bridge on top of them. An upper carriage with a forestry crane can move along the bridge. A system is proposed that estimates the position of the carriage. The Extended Kalman Filter (EKF) handles the non-linearity of the system and provides information about the uncertainty of the state estimation. The load on the hydraulically actuated legs is different for every carriage position on top of the mechanism. We assume that the dynamic effects of the movement can be modeled with a linear model. The state is described by the position, velocity, and acceleration of the center of gravity of the machine's upper carriage. The non-linear relation between the state vector and the pressures in the hydraulic actuators is linearized in the innovation step of the applied filter. The proposed system is evaluated in a multibody machine simulation with hydraulic co-simulation. The proposed system reduces the number of required sensors on this type of walking forestry machine as the movements do not need to be captured directly. The results show that modern state estimation and prediction can support predictive control of complex, dynamic hydraulically driven systems.

Keywords: Extended Kalman Filter, state estimation, system simulation, portal advancing mechanism

1 Introduction

The forestry industry is gaining international recognition among the general public as a producer of wood used as a climate-friendly building material or a carbon-neutral energy source [1, 2]. Sustainable forestry operations are a key factor to live up to the public interests. As a consequence, conserving forest soils is critical because they are the primary resource for long-term forest growth. Soil damage on the other hand has a negative impact on the overall productivity of a forest [3, 4].

In today's fully mechanized harvesting operations, the soil gets damaged through the machine weight, which can reach up to 30 t, and wheel slip [5]. To reduce soil damage induced by state-of-the-art forestry machines, new machine types are subject to current research activities [6, 7]. Machines that are non-wheel driven have a high potential in reducing soil damage by avoiding wheel slip. Having said this, legged machine types that reduce the slip to zero require smart control systems to ensure stability and safety [8]. In addition to that, the automation of state-of-the-art machines is currently under development to use its potential to support the driver in their challenging tasks [9, 10]. As well automation is seen as one of the keys to increase the overall productivity of forestry machines and help these machines to become even more environmentally friendly [9, 11, 12].

In hydraulic actuated systems, it is hard to achieve guaranteed control performance because of the nontrivial control challenge due to non-linear friction, deadbands, etc. [11, 13]. To ensure stability in an automated working

or walking process active control is needed. Therefore knowledge of the current and a possible future state of the machine is required [8]. The state could be observed by motion sensors. But to get an accurate measurement, these sensitive sensors have to be placed in positions where they can be easily damaged or influenced e.g. by debris.

In this article, we investigate the portal advancing mechanism, a machine with a walking frame and an upper carriage on top of it. The objective is to estimate the state of the upper carriage without the use of expensive and easily damaged motion sensors. Because of changes in acceleration, a linear movement model based on the kinetic movement equation with constant acceleration will not achieve an accurate state. Here, rather cheap pressure sensors can be used to provide information about the state. This is possible because every position of the upper carriage's center of mass introduces a different load to the hydraulic actuators. A non-linear model that can be easily linearized describes the relationship between pressures and machine state.

In a first step a simulation is used to generate the necessary data to test this approach. With these data an Extended Kalman Filter (EKF) can be set up to predict the machines state based on the movement and measurement model. To handle non-linear systems the EKF uses a linearization around the working point [14]. The EKF improves the prediction of the state from the movement model by the use of measurement data, that are linked to the state through the measurement model. Additionally the covariance matrix quantifies the uncertainty of the prediction and therefore, can quantify the reliability of the estimation. Through the utilization of the simulated measurement data a better knowledge of the state is gained with reduced uncertainty.

The article is organized as follows. In section 2 the system is described and a measurement model is derived. After that in section 3 the filter design with the EKF is presented. In section 4 the results of the prediction are show in comparison to the simulation data and in section 5 the results are summarized in the conclusion.

2 System Description

2.1 Portal Advancing Mechanism

The portal advancing mechanism realizes a legged, non-bionic principle for locomotion on sensitive soils. The mechanism was first presented in [15] as part of the development of the so-called *Portalharvester*. The frame consists of two bases, which are held in place by three hydraulically actuated legs each, and a bridge connecting the bases, as can be seen in fig. 1. A carriage with the work functions and the power delivery unit placed on top of the bridge can drive along the bridge. At each base, the bridge's inclination can be adjusted to account for the terrain's slope. The portal advancing mechanism moves over terrain with nearly zero slip, and the overall affected area by the machine is minimized in comparison to classical forestry machinery. [15]

Figure 1: Rendering of the Portal Advancing Mechanism with a forestry crane [15]

In this study, only the movement of the upper carriage is of interest. The upper carriage is assumed to be equipped with a forestry crane. In addition to the linear motion along the bridge of the carriage, the upper carriage can be rotated by 360 degrees and extend its crane.

2.2 Development of the Measurement Model

The pressure in the chambers of the hydraulic cylinders p_{piston_i} and p_{rod_i} of each leg changes depending on the load the upper carriage introduces to the movement mechanism. To estimate the position of the upper carriage's

center of gravity, it is necessary to develop a model that describes the relationship between the position of the upper carriage's center of gravity and the pressures in the hydraulic system. This is explained in the following section. The model for the estimation approach is based on the equilibrium of forces and torques of the portal advancing mechanism. The following figures are used (fig. 2 & fig. 3) to derive the required equations. This includes all acting forces and points of attack for the movement mechanism in a simplified way. This model allows no movement in the z-direction of the point mass which is used as a simplified model of the upper carriage.

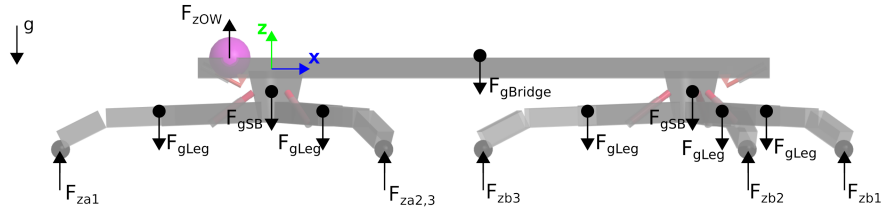

Figure 2: Side view of the mechanism in the x-z plane

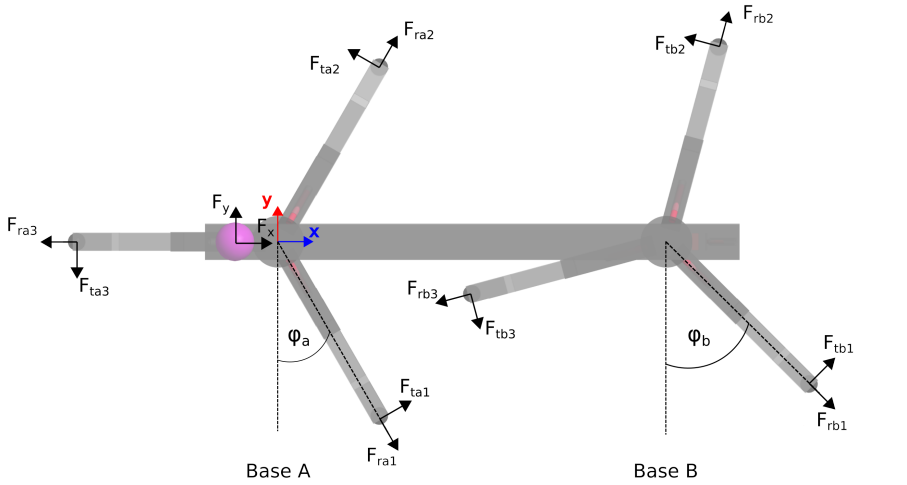

Figure 3: Top view of the mechanism in the x-y plane.

Based on the the forces and points of attack the equilibrium of forces can be established. A description of all forces is given in tab. 1.

Table 1: Definition of the forces, where $i \in [a,b]$ and $j \in [1,2,3]$.

Force	Description
F_x	inertia force of the upper carriage in x-direction
F_y	inertia force of the upper carriage in y-direction
F_z	inertia and weight force of the upper carriage in z-direction
F_{gSB}	weight force of the body of a base
F_{gLeg}	weight force of a leg
$F_{gBridge}$	weight force of the bridge
$F_{r\{i,j\}}$	ground contact force along the leg axis
$F_{t\{i,j\}}$	ground contact force tangential to the leg axis
$F_{z\{i,j\}}$	vertical ground contact force

For the derivation of the measurement model it is necessary to transfer the forces at the end of each leg, given in

fig. 3, into the $\{x,y,z\}$ coordinate system. This is done by the following conversion:

$$\boldsymbol{F_{Leg}}_{\{x,y,z\}} = \begin{pmatrix} sin(\varphi_j + (i-1)\frac{2}{3}\pi) & -cos(\varphi_j + (i-1)\frac{2}{3}\pi) & 0 \\ cos(\varphi_j + (i-1)\frac{2}{3}\pi) & sin(\varphi_j + (i-1)\frac{2}{3}\pi) & 0 \\ 0 & 0 & 1 \end{pmatrix} \begin{pmatrix} F_{r\{i,j\}} \\ F_{t\{i,j\}} \\ F_{z\{i,j\}} \end{pmatrix} \tag{1}$$

where $i \in [a,b]$ and $j \in [1,2,3]$.
With that, the equilibrium of forces in the $\{x,y,z\}$ coordinate system can be used:

$$\boldsymbol{0} = \sum_i \boldsymbol{F_i}_{\{x,y,z\}}. \tag{2}$$

This yields the first three equations for our model.

For the equilibrium of torques the coordinate origin over the left base is used as reference point, see fig. 2 & fig. 3. This point is positioned in the plane, where the movement of the point mass of the upper carriage is modeled. Furthermore, this point lies in the rotational axis of the base underneath. With this positioning of the reference axes for the equilibrium of torques the distances can be defined. A description of all used distances is given in tab. 2.

Table 2: Definition of the position, angles and distances.

Variable	Description	Value
$(x,y,z)^T$	upper carriage position in the $\{x,y,z\}$ coordinate system	
φ_a	rotation of the left base around the z-axis	$-\frac{\pi}{2}$
φ_b	rotation of the right base around the z-axis	0
l_{Leg}	length of a leg, relative to the z-axis of a base	3.112 m
l_{gLeg}	position of the leg's center of mass, relative to the z-axis of a base	1.935 m
l_{Bridge}	distance between rotational axis of the two bases	6 m
h_{SB}	height of the movement plane of the upper carriage model	1.467 m
a_1	displacement in x direction of the base's connecting bolt	0.18 m
b_1	displacement in z direction of the base's connecting bolt	0.372 m

With these definitions we can calculate the Torques around the origin of the coordinate System for all acting forces as follows:

$$\begin{aligned}
\boldsymbol{T_{gLeg,a,i}} &= \begin{pmatrix} l_{gLeg}sin(\varphi_a + (i-1)\frac{2}{3}\pi) \\ -l_{gLeg}cos(\varphi_a + (i-1)\frac{2}{3}\pi) \\ 0 \end{pmatrix} \times \begin{pmatrix} 0 \\ 0 \\ -F_{gLeg} \end{pmatrix}, && i \in [1,2,3] \\
\boldsymbol{T_{gLeg,b,i}} &= \begin{pmatrix} l_{gLeg}sin(\varphi_b + (i-1)\frac{2}{3}\pi) + l_{Bridge} \\ -l_{gLeg}cos(\varphi_b + (i-1)\frac{2}{3}\pi) \\ 0 \end{pmatrix} \times \begin{pmatrix} 0 \\ 0 \\ -F_{gLeg} \end{pmatrix}, && i \in [1,2,3] \\
\boldsymbol{T_{gBridge}} &= \begin{pmatrix} \frac{l_{Bridge}}{2} \\ 0 \\ 0 \end{pmatrix} \times \begin{pmatrix} 0 \\ 0 \\ -F_{gBridge} \end{pmatrix} \\
\boldsymbol{T_{gSB}} &= \begin{pmatrix} l_{Bridge} \\ -\frac{h_{SB}}{3} \\ 0 \end{pmatrix} \times \begin{pmatrix} 0 \\ 0 \\ -F_{gSB} \end{pmatrix} \\
\boldsymbol{T_{F_{Leg,a,i}}} &= \begin{pmatrix} l_{Leg}sin(\varphi_a + (i-1)\frac{2}{3}\pi) \\ -l_{Leg}cos(\varphi_a + (i-1)\frac{2}{3}\pi) \\ -h_{SB} \end{pmatrix} \times \begin{pmatrix} F_{x,a,i} \\ F_{y,a,i} \\ F_{z,a,i} \end{pmatrix}, && i \in [1,2,3] \\
\boldsymbol{T_{F_{Leg,b,i}}} &= \begin{pmatrix} l_{Leg}sin(\varphi_b + (i-1)\frac{2}{3}\pi) + l_{Bridge} \\ -l_{Leg}cos(\varphi_b + (i-1)\frac{2}{3}\pi) \\ -h_{SB} \end{pmatrix} \times \begin{pmatrix} F_{x,b,i} \\ F_{y,b,i} \\ F_{z,b,i} \end{pmatrix}, && i \in [1,2,3].
\end{aligned} \tag{3}$$

With that the equilibrium of torque is:

$$\boldsymbol{0} = \boldsymbol{T_{gSB}} + \boldsymbol{T_{gBridge}} + \sum_{i=1}^{3} \left[\boldsymbol{T_{gLeg,a,i}} + \boldsymbol{T_{gLeg,b,i}} + \boldsymbol{T_{F_{Leg,a,i}}} + \boldsymbol{T_{F_{Leg,b,i}}} \right] \tag{4}$$

.

This results in 6 equations with 18 variables, 6 vertical ground forces $F_{z,a,i}$ and $F_{z,b,i}$ and 12 forces in the ground plane $F_{x,a,i}$, $F_{x,b,i}$, $F_{y,a,i}$ and $F_{y,b,i}$. This system of equations does not yield a clear solution. Therefore, in the next section, additional conditions are introduced to the system.

2.3 Additional Conditions for the Measurement Model

For the system to yield a clear solution additional equations are required. The free cut of one base shows, that the torque around the z-axis has to be zero. The connection between bridge and base can not transfer any torque. This leads to two equations, one for each base:

$$\sum_j \boldsymbol{T}_{\boldsymbol{F}_{\boldsymbol{Leg},i,j}} = \begin{pmatrix} T_{j,x} \\ T_{j,y} \\ 0 \end{pmatrix}, \qquad i \in [a,b] \;\; j \in [1,2,3]. \tag{5}$$

A similar set of conditions result from the actuators at each base, which are used to control the inclination of the bridge. The valve is in a floating position that both sides of the cylinders are connected to tank when all legs are on the ground. Therefore, they do not exert any force. With no exerted force, the torque around the bolt connecting the base and the bridge in the y-axis is zero. With this condition two additional equations are gained.

$$\begin{aligned} \begin{pmatrix} T_{connector,a,x} \\ 0 \\ T_{connector,a,z} \end{pmatrix} = & \begin{pmatrix} l_{Leg} sin(\varphi_a + (i-1)\frac{2}{3}\pi) - a_1 \\ l_{Leg} cos(\varphi_a + (i-1)\frac{2}{3}\pi) \\ -h_{SB} + b_1 \end{pmatrix} \times \begin{pmatrix} F_{x,b,i} \\ F_{y,b,i} \\ F_{z,b,i} \end{pmatrix} \\ & + \begin{pmatrix} l_{gLeg} sin(\varphi_a + (i-1)\frac{2}{3}\pi) - a_1 \\ l_{gLeg} cos(\varphi_a + (i-1)\frac{2}{3}\pi) \\ -\frac{h_{SB}}{3} + b_1 \end{pmatrix} \times \begin{pmatrix} 0 \\ 0 \\ -F_{gLeg} \end{pmatrix} \\ & + \begin{pmatrix} -a_1 \\ 0 \\ -\frac{h_{SB}}{3} + b_1 \end{pmatrix} \times \begin{pmatrix} 0 \\ 0 \\ -F_{gSB} \end{pmatrix}, \qquad i \in [1,2,3]. \end{aligned} \tag{6}$$

$$\begin{aligned} \begin{pmatrix} T_{connector,b,x} \\ 0 \\ T_{connector,b,z} \end{pmatrix} = & \begin{pmatrix} l_{Leg} sin(\varphi_b + (i-1)\frac{2}{3}\pi) + a_1 \\ l_{Leg} cos(\varphi_b + (i-1)\frac{2}{3}\pi) \\ -h_{SB} + b_1 \end{pmatrix} \times \begin{pmatrix} F_{x,b,i} \\ F_{y,b,i} \\ F_{z,b,i} \end{pmatrix} \\ & + \begin{pmatrix} l_{gLeg} sin(\varphi_b + (i-1)\frac{2}{3}\pi) + a_1 \\ l_{gLeg} cos(\varphi_b + (i-1)\frac{2}{3}\pi) \\ -\frac{h_{SB}}{3} + b_1 \end{pmatrix} \times \begin{pmatrix} 0 \\ 0 \\ -F_{gLeg} \end{pmatrix} \\ & + \begin{pmatrix} a_1 \\ 0 \\ -\frac{h_{SB}}{3} + b_1 \end{pmatrix} \times \begin{pmatrix} 0 \\ 0 \\ -F_{gSB} \end{pmatrix}, \qquad i \in [1,2,3]. \end{aligned} \tag{7}$$

For the next equation the following assumption is made: It is assumed that the torque of the bridge around the x-axis is split equally between the bases. Therefore the torques $(T_{a,x}, T_{a,y}, 0)^T$ and $(T_{b,x}, T_{b,y}, 0)^T$ of the bases have to be equal in the x-axis.

$$T_{a,x} = T_{b,x} \tag{8}$$

A further assumption is made for the next equation. Similar to the equal torques in eq. (8) it is assumed that the forces along the bridge axis (x-axis) are distributed in an equal way between the bases. Therefore, the sums of the forces in the x-direction of each base have to be equal:

$$\sum_{i=1}^{3} F_{x,a,i} = \sum_{i=1}^{3} F_{x,b,i} \tag{9}$$

With these additional equations (eq. (5) - (9)) the system consists of 12 equations with 18 variables.
In a previous work [7] a method to calculate the vertical ground force of a leg based on the hydraulic pressures is presented. For this the following assumption is made: It is assumed that the planar ground force F_r of each leg is zero. It was shown, that this assumption leads only to small errors in the calculation of the ground force of a leg. Thus the system can be reduced by 6 variables and a analytical solution for the system with 12 equations and 12

variables can be found. The system yields non-linear solutions for $F_{t,i,j}$ and $F_{z,i,j}$, depending on the position and the acceleration of the upper carriage.

The relation between the measurement value and the ground force derived in [7] is as follows

$$F_{z_i} = \frac{(l_r sin(\alpha_{cylinder}) - l_z cos(\alpha_{cylinder}) p_i A_{piston} + l_{gLeg} F_{gLeg}}{l_{Leg}}. \tag{10}$$

Hereby $\alpha_{cylinder}$ is the angle the cylinder stands relative to the ground plane, l_r and l_z are geometrical values. In this formula there is only a the pressure term for the force the hydraulic cylinder exerts, the influence of friction on the exerted force of the cylinder is neglected for simplification purposes. To describe the measurements in a more general way, a further simplification is also added. The pressures in the chambers of the cylinders are recalculated to single pressures with:

$$p_i = p_{piston_i} - \frac{A_{rod}}{A_{piston}} p_{rod_i}, \qquad i \in [a_1, a_2, a_3, b_1, b_2, b_3], \tag{11}$$

where A_{rod} describes the area on the rod side of the cylinder and A_{piston} the area on the piston side. With the analytical solution for $F_{z,i,j}$ and eq. 10 the individual pressures can be calculated. Therefore we insert directly the geometrical constants that are given in tab. 2 and get the following solutions for the simplified pressures for each leg cylinder. These pressures depend on the weight forces of the mechanism and the position and acceleration of the upper carriage:

$$\begin{aligned} p_{a,1} = \frac{1}{A_{piston}} \Big[& 2.743376955 F_{gLeg} + 0.9998181642 F_{gBridge} + 2.261264199 F_{gSb} + 0.3545454477 \\ & (-7000.0 a_z - 68670.0) y + 14444.18157 a_z + 141697.4211 - 1.386448847 \cdot 10^{-10} \\ & (-7000.0 a_z - 68670.0) x + 2481.818130 a_y z + 6493.729699 a_y + 6.363226316 \cdot 10^{-9} a_x \\ & - 3.667828308 \cdot 10^{-7} a_x z - 3.673810426 \cdot 10^{-7} a_x y \Big] \end{aligned} \tag{12}$$

$$\begin{aligned} p_{a,2} = \frac{1}{A_{piston}} \Big[& 2.743376923 F_{gLeg} + 1.196039067 F_{gBridge} + 2.261264197 F_{gSB} + 0.4241273283 \\ & (-7000.0 a_z - 68670.0) y + 17278.94738 a_z + 169506.4737 - 0.6293788332 \\ & (-7000.0 a_z - 68670.0) x + 2968.891299 a_y z - 1680.819113 a_y - 12926.18247 a_x \\ & - 4405.651825 a_x z - 2154.363747 a_y x + 2154.363747 a_x y \Big] \end{aligned} \tag{13}$$

$$\begin{aligned} p_{a,3} = \frac{1}{A_{piston}} \Big[& F_{gLeg} + 1.196039068 F_{gBridge} + 2.261264197 F_{gSB} + 0.4241273283 \\ & (-7000.0 a_z - 68670.0) y + 17278.94739 a_z + 169506.4738 + 0.6293788343 \\ & (-7000.0 a_z - 68670.0) x + 2968.891301 a_y z - 1680.819114 a_y + 12926.18248 a_x \\ & + 4405.651832 a_x z + 2154.363747 a_y x - 2154.363747 a_x y \Big] \end{aligned} \tag{14}$$

$$\begin{aligned} p_{b,1} = \frac{1}{A_{piston}} \Big[& 2.743376944 F_{gLeg} - 4955.777018 + 1.130632097 F_{gBridge} + 2.261264194 F_{gSB} \\ & - 505.1760471 a_z - 0.7267440767 (-7000.0 a_z - 68670.0) x - 2806.533569 a_y z \\ & - 1044.030492 a_y + 1.845335632 \cdot 10^{-6} a_x - 5087.208545 a_x z - 0.4009333684 \\ & (-7000.0 a_z - 68670.0) y + 2487.644979 a_y x - 2487.644979 a_x y \Big] \end{aligned} \tag{15}$$

$$\begin{aligned} p_{b,2} = \frac{1}{A_{piston}} \Big[& 2.743376923 F_{gLeg} + 1.017343910 F_{gBridge} + 2.261264197 F_{gSB} - 0.3607602514 \\ & (-7000.0 a_z - 68670.0) y - 454.5579174 a_z - 4459.213167 + 0.3633720387 \\ & (-7000.0 a_z - 68670.0) x - 2525.321756 a_y z - 5763.608456 a_y \\ & - 1.209013000 \cdot 10^{-6} a_x + 2543.604273 a_x z - 1243.822489 a_y x + 1243.822488 a_x y \Big] \end{aligned} \tag{16}$$

$$
\begin{aligned}
p_{b,3} = \frac{1}{A_{piston}} \Big[& 2.743376948 F_{gLeg} + 1.243920287 F_{gBridge} + 2.261264199 F_{gSB} - 0.4411064850 \\
& (-7000.0 a_z - 68670.0) y - 555.7941719 a_z - 5452.340826 + 0.3633720382 \\
& (-7000.0 a_z - 68670.0) x - 3087.745398 a_y z + 3675.547470 a_y \\
& - 1.908967895 \cdot 10^{-7} a_x + 2543.604273 a_x z - 1243.822489 a_y x + 1243.822489 a_x y \Big]
\end{aligned} \tag{17}
$$

2.4 Inertial measurement unit

In many vehicle applications inertial measurement units (IMUs) are used for velocity and position estimation when the velocity or the position can not be measured directly, or can not be measured with the required frequency. The measured acceleration is integrated over time to determine the position and velocity. Compared to direct measurements the disadvantage of IMUs is, that the measurement noise is also integrated over time. An IMU can not be used directly to measure the position of the center of mass of the upper carriage on the portal advancing mechanism. When the crane of the upper carriage is moving, the center of mass of the upper carriage also moves. If, however, two or more IMUs are used which measure the movement of the upper carriage and the movement of the crane, the center of mass and the corresponding acceleration can be calculated. In this case, the mass of gripped objects has to be neglected or estimated by other sensors. In the following we use the corresponding acceleration a_x, a_y, a_z which are located in the center of mass of the upper carriage and benchmark this system as alternative to our estimator or position sensors.

3 Filter design

The upper carriage is reduced to a point mass with equivalent forces, to facilitate the filter design. The filter's objective is to estimate the upper carriage's position and velocity. The movement of the upper carriage is modeled as a linear time-invariant system with state $\boldsymbol{x}_k$ and time index k. The state vector has nine dimensions,

$$
\boldsymbol{x} = [x, y, z, v_x, v_y, v_z, a_x, a_y, a_z]^T, \tag{18}
$$

where x, y, z are the corresponding coordinates of the upper carriage's position in the local machine coordinate system, v_x, v_y, v_z the speed of the carriage in every direction, and the corresponding accelerations a_x, a_y, a_z. The described system is observed by a linear estimator with the estimated state $\boldsymbol{x}_k$ at time t_k and the estimation covariance $\mathbf{P}_k$. The implemented Extended Kalman-Filter estimator [16] consist of two steps, state prediction and update.

1) Prediction step:

The next system state $\boldsymbol{x}^p_{k+1}$ is predicted based on the last known estimation $\boldsymbol{x}_k$. For the prediction of the system state, a linear constant acceleration model was used

$$
\boldsymbol{x}^p_{k+1} = \mathbf{A}\boldsymbol{x}_k + \omega_k \tag{19}
$$

with time-interval dt and the system matrix $\mathbf{A}$ as

$$
A = \begin{bmatrix}
1 & 0 & 0 & dt & 0 & 0 & \frac{dt^2}{2} & 0 & 0 \\
0 & 1 & 0 & 0 & dt & 0 & 0 & \frac{dt^2}{2} & 0 \\
0 & 0 & 1 & 0 & 0 & dt & 0 & 0 & \frac{dt^2}{2} \\
0 & 0 & 0 & 1 & 0 & 0 & dt & 0 & 0 \\
0 & 0 & 0 & 0 & 1 & 0 & 0 & dt & 0 \\
0 & 0 & 0 & 0 & 0 & 1 & 0 & 0 & dt \\
0 & 0 & 0 & 0 & 0 & 0 & 1 & 0 & 0 \\
0 & 0 & 0 & 0 & 0 & 0 & 0 & 1 & 0 \\
0 & 0 & 0 & 0 & 0 & 0 & 0 & 0 & 1
\end{bmatrix}. \tag{20}
$$

The deviation between the real state and our prediction $\boldsymbol{x}^p_{k+1}$ is expressed by unknown the noise value ω_k. We assume that the expected value $E[\omega_k]$ of the noise is zero and that the noise is normally distributed (Gaussian distribution). The resulting covariance $\mathbf{P}^p_{k+1}$ is predicted as

$$
\mathbf{P}^p_{k+1} = \mathbf{A}\mathbf{P}_k\mathbf{A}^T + \mathbf{Q} \tag{21}
$$

with system noise $\mathbf{Q}$. The system noise $\mathbf{Q}$ is the covariance of the noise value $\mathbf{Q} = Cov(\omega_k)$. We assumed an uncorrelated noise with the following variances,

$$\mathbf{Q} = \begin{bmatrix} 0.0025 & 0 & 0 & 0 & 0 & 0 & 0 & 0 & 0 \\ 0 & 0.0025 & 0 & 0 & 0 & 0 & 0 & 0 & 0 \\ 0 & 0 & 0.0025 & 0 & 0 & 0 & 0 & 0 & 0 \\ 0 & 0 & 0 & 2.5E-5 & 0 & 0 & 0 & 0 & 0 \\ 0 & 0 & 0 & 0 & 2.5E-5 & 0 & 0 & 0 & 0 \\ 0 & 0 & 0 & 0 & 0 & 2.5E-5 & 0 & 0 & 0 \\ 0 & 0 & 0 & 0 & 0 & 0 & 0.0013 & 0 & 0 \\ 0 & 0 & 0 & 0 & 0 & 0 & 0 & 0.0013 & 0 \\ 0 & 0 & 0 & 0 & 0 & 0 & 0 & 0 & 0.0013 \end{bmatrix}. \tag{22}$$

2) Update step:

In the second step, the predicted state $\boldsymbol{x}_k^p$ with covariance $\mathbf{P}_k^p$ is updated with the current time-step's measurement $\boldsymbol{z}_k$. The measurement vector $\boldsymbol{z}_k$ consists of the pressure measurements of all six cyclinders and the transformed inertia measurements,

$$\boldsymbol{z}_k = [p_{a1}, p_{a2}, p_{a3}, p_{b1}, p_{b2}, p_{b3}, a_x, a_y, a_z]^T, \tag{23}$$

Additionally there was a constant bias $\boldsymbol{x}_o$ of the measurement model which was added to the system state as,

$$\boldsymbol{z}_k = \hat{\boldsymbol{h}}(\boldsymbol{x}_k) = \boldsymbol{h}(\boldsymbol{x}_k + \boldsymbol{x}_o) \tag{24}$$

where

$$\boldsymbol{x}_o = [0.08, 0, 0, 0, 0, 0, 0.5, 0, 0]^T, \quad \frac{\boldsymbol{x}_o}{\boldsymbol{\delta x}} = \boldsymbol{0}.$$

The measurement noise $\mathbf{R}$ consists of the model noise $\mathbf{R}_{model}$, which is due to the error of the measurement model, and the sensor noise $\mathbf{R}_{sensor}$. Both are modeled as normally distributed noise and are characterized by their covariance. The sensor noise was assumed to be non correlated with a standard deviation of $\sigma_p = 1\ bar$ for the pressure sensors and $\sigma_i = 0.20\ \frac{m}{s^2}$ for the inertial measurement unit. The variance of the model noise was assumed to be equal to the cross covariance of the simulated pressure values $\boldsymbol{p}_i^{sim}$ and the corresponding pressure values calculated with the measurement model $\boldsymbol{p}_i^{model}$. Given the time series $k = 1...n$, the coefficients of the cross covariance are calculated as,

$$R_{ij} = \sum_{k=1}^{n} \left[(p_i^{sim} - p_i^{model})(p_j^{sim} - p_j^{model}) \right]_k, \quad i, j \in [a_1, a_2, a_3, b_1, b_2, b_3], \tag{25}$$

see Appendix A, eq. (33).

In consequence, the added measurement noise is,

$$\mathbf{R} = \mathbf{R}_{model} + \mathbf{R}_{sensor}$$
$$= \begin{bmatrix} R_{a1a1} + \sigma_p^2 & R_{a1a2} & R_{a1a3} & R_{ab1} & R_{a1b2} & R_{a1b3} & 0 & 0 & 0 \\ R_{a2a1} & R_{a2a2} + \sigma_p^2 & R_{a2a3} & R_{a2b1} & R_{a2b2} & R_{a2b3} & 0 & 0 & 0 \\ R_{a3a1} & R_{a3a2} & R_{a3a3} + \sigma_p^2 & R_{a3b1} & R_{a3b2} & R_{a3b3} & 0 & 0 & 0 \\ R_{b1a1} & R_{b1a2} & R_{b1a3} & R_{b1b1} + \sigma_p^2 & R_{b1b2} & R_{b1b3} & 0 & 0 & 0 \\ R_{b2a1} & R_{b2a2} & R_{b2a3} & R_{b2b1} & R_{b2b2} + \sigma_p^2 & R_{b2b3} & 0 & 0 & 0 \\ R_{b3a1} & R_{b3a2} & R_{b3a3} & R_{b3b1} & R_{b3b2} & R_{b3b3} + \sigma_p^2 & 0 & 0 & 0 \\ 0 & 0 & 0 & 0 & 0 & 0 & \sigma_i^2 & 0 & 0 \\ 0 & 0 & 0 & 0 & 0 & 0 & 0 & \sigma_i^2 & 0 \\ 0 & 0 & 0 & 0 & 0 & 0 & 0 & 0 & \sigma_i^2 \end{bmatrix}. \tag{26}$$

The Kalman Filter requires a linear measurement model to calculate the postori covariances. The measurement model of the studied system is, however, non-linear, see Section 2.2. Therefore, the Extended Kalman-Filter is applied, which requires a linearization of the measurement model. The predicted system state $\boldsymbol{x}_k^p$ is used as a linearization point. The Jacobian matrix of the measurement model $\mathbf{H}$ is calculated at the predicted system state,

$$\mathbf{H}(\boldsymbol{x}_k) = \frac{\partial \boldsymbol{h}(\boldsymbol{x})}{\partial \boldsymbol{x}}\Big|_{\boldsymbol{x}=\boldsymbol{x}_k^p} \tag{27}$$

The partial derivatives lead to the Jacobian as,

$$\mathbf{H}(\boldsymbol{x}_k^p) = \begin{bmatrix} \frac{p_{a,1}}{\delta x}(a_z) & \frac{p_{a,1}}{\delta y}(a_z) & 0 & 0 & 0 & 0 & \frac{p_{a,1}}{\delta a_x}() & \frac{p_{a,1}}{\delta a_y}() & \frac{p_{a,1}}{\delta a_z}(x,y) \\ \frac{p_{a,2}}{\delta x}(a_y,a_z) & \frac{p_{a,2}}{\delta y}(a_x,a_z) & 0 & 0 & 0 & 0 & \frac{p_{a,2}}{\delta a_x}(y) & \frac{p_{a,2}}{\delta a_y}(x) & \frac{p_{a,2}}{\delta a_z}(x,y) \\ \frac{p_{a,3}}{\delta x}(a_y,a_z) & \frac{p_{a,3}}{\delta y}(a_x,a_z) & 0 & 0 & 0 & 0 & \frac{p_{a,3}}{\delta a_x}(y) & \frac{p_{a,3}}{\delta a_y}(x) & \frac{p_{a,3}}{\delta a_z}(x,y) \\ \frac{p_{b,1}}{\delta x}(a_y,a_z) & \frac{p_{b,1}}{\delta y}(a_x,a_z) & 0 & 0 & 0 & 0 & \frac{p_{b,1}}{\delta a_x}(y) & \frac{p_{b,1}}{\delta a_y}(x) & \frac{p_{b,1}}{\delta a_z}(x,y) \\ \frac{p_{b,2}}{\delta x}(a_y,a_z) & \frac{p_{b,2}}{\delta y}(a_x,a_z) & 0 & 0 & 0 & 0 & \frac{p_{b,2}}{\delta a_x}(y) & \frac{p_{b,2}}{\delta a_y}(x) & \frac{p_{b,2}}{\delta a_z}(x,y) \\ \frac{p_{b,3}}{\delta x}(a_y,a_z) & \frac{p_{b,3}}{\delta y}(a_x,a_z) & 0 & 0 & 0 & 0 & \frac{p_{b,3}}{\delta a_x}(y) & \frac{p_{b,3}}{\delta a_y}(x) & \frac{p_{b,3}}{\delta a_z}(x,y) \end{bmatrix}, \tag{28}$$

where $\frac{p_{a,1}}{\delta a_x}()$ and $\frac{p_{a,1}}{\delta a_y}()$ are constant.

The Kalman gains determine the influence of the new measurement in relation to the state prediction and are calculated as,

$$\mathbf{K}_k = \mathbf{P}_k^p \mathbf{H}_k^T \left(\mathbf{H}_k \mathbf{P}_k^p \mathbf{H}_k^T + \mathbf{R}\right)^{-1}. \tag{29}$$

The innovation $\boldsymbol{y}_k$ is the evaluation of the measurement compared to the assumed measurement of the predicted system state. In this case no linearization is required and the non-linear measurement model is directly applied and the innovation follows as

$$\boldsymbol{y}_k = \boldsymbol{z}_k - \hat{\boldsymbol{h}}(\boldsymbol{x}_k^p). \tag{30}$$

Finally, the state update is

$$\boldsymbol{x}_k = \boldsymbol{x}_k^p + \mathbf{K}_k \boldsymbol{y}_k \tag{31}$$

with the state covariance updated accordingly

$$\mathbf{P}_k = \mathbf{P}_k^p - (\mathbf{K}_k \mathbf{H}_k \mathbf{P}_k^p). \tag{32}$$

4 Simulation Results

4.1 Simulative Load Cycles

The mechanism is currently in an early stage of development, and no real-world prototype exists to collect data that could be used to test the estimation method presented in this article. As a consequence, a coupled simulation is used to generate the necessary test data. The model used in a previous work [7] is modified to meet the needs. This simulation model is made up of two different models, the multi-body model, which inherits all bodies and kinematics, and a model of the hydraulic drive train. All predicted key masses of the mechanism are given in tab. 3. To reduce complexity and to increase computing efficiency only the cylinders, that hold the legs in place,

Table 3: Masses of the individual bodies

Body	Mass
Upper Carriage	7000 kg
Bridge	2172 kg
Base	855 kg
Leg	462 kg

were modeled in the hydraulic model. For the movement of the other actuators it can be assumed that there will be no motion or small movements, but no hydraulic forces exerted. Therefore, they were not modeled hydraulically and set to a rigid distance or a force free joint in the multi-body model.

To further simplify the model, the upper carriage is modeled as a single point mass on the bridge, as can be seen in fig. 2 & fig. 3 as a pink ball. A further simplification is added to the model: The movement of the combined center of mass is reduced to a planar movement in the x-y-plane and therefore, no movement in the z-axis is implemented. By the reduction of the upper carriage to one single mass, the movement had to be controlled in a different way than by hydraulically modeled actuators. Simple time dependent signals are used for the velocity of the joints needed for the planar movement. To generate a more realistic behavior in the acceleration the velocity signal was delayed by a transfer function with PT1-behavior. With this adapted and simplified model data for the movement of the mechanisms upper carriage center of mass were generated.

Five different movement cycles are created with this simulation, that reflect possible movements of the center of mass of the upper carriage while using the crane. They all include movements along the bridge axis, perpendicular to the bridge and movements that resemble the rotation of the upper carriage. Here, the perpendicular movements create a similar movement of the center of mass as the crane's extension and retraction. Each movement cycle is individual in shape. One cycle features a movement around the whole bridge, the other four start at one end of the bridge and end at the other end. These four cycles have a different number of movements, which resemble the movement of the crane and upper carriage. They range from one to three extensions and retractions with different overlapping of the linear and rotation movement of the upper carriage..

In this first step the gripping and lifting of a tree is not considered, because the load of a tree can not easily be estimated. The grip of a tree would have a great influence on the position of the center of mass and the mass itself. With that the estimation would be invalid, because the masses of the load is not introduced in the measurement model (see. eq. 12-17).

4.2 Estimator results

Figure 4 shows the estimation analysis for the fifth test cycle. The performance of the presented combination of the EKF estimator with additional IMU measurements was compared to that of an IMU system and the estimator without IMU measurements. The IMU system was very robust in terms of acceleration. Otherwise, however, it lacked stationary precision as the IMU noise is integrated over time. The estimator is able to estimate the position to a certain tolerance. Along the bridge (x-axis), the deviation of the position estimation was slightly higher than that perpendicular to the bridge. The velocity and acceleration accuracy were the other way around, with slightly increased deviations perpendicular to the bridge than along the bridge. Especially the acceleration in y-direction shows significant systematic errors, see Figure 4d. The integration of the IMU measurements into the estimator had virtually no effect on the estimation results. A slight decrease in the deviation in the velocity and acceleration estimations was noted. In contrast to the IMU, which integrates the acceleration measurements to determine the velocity, the estimator determines the velocity implicitly as the relation between the position and the velocity is modeled in the system model.

Each cycle was repeated five times to evaluate the estimators overall standard deviation. The 75% and 95% confidence interval of all runs for the five cycles are plotted in Figure 5a. For all cycles, the positions estimates are characterized by a high accuracy, the maximum outlier error is less then 0.3m with an confidence error of less then 0.2m in the 75% confidence interval and typical errors of less then 0.1m. However it can be remarked, that the standard deviation of the position along the machine axis (σ_x) is considerably higher than in the perpendicular axis (σ_y), see Figure 5.

4.3 Discussion

The primary objective of the application of a state estimator was to avoid the necessity for position sensors. The required precision has to be determined by the intended application. Clearly, IMUs can not be used to obtain a reliable estimation of the center of mass' position and is no alternative to position sensors or the proposed estimator. For the envisaged tasks, the achieved accuracy of the estimator is sufficient to ensure stability of the legged mechanism without additional position sensors. Even when using position sensors, the proposed system offers an additional information source and additional redundancy, which is especially important given the harsh environment of such sensors. Nevertheless, an accurate acceleration and velocity estimation is important when model predictive control comes into play. Especially along the y-axis, the estimation showed a low accuracy. It has to be evaluated if the achieved accuracy is sufficient based on the actual control requirements. A more complex measurement and system model could increase the accuracy of the velocity and acceleration estimates. Here, the implementation of a cylinder friction model could have a positive effect on the estimation, since the approach is based on the force exerted by the cylinders. In the current state not the actual force is used for the estimation, because the friction is neglected. A more sophisticated model should also integrate the control signals of the system, for example, the requested movement of the upper carriage. However, external influences on the upper carriage mass point, for example, gripped trees, can not be predetermined and therefore have to be accounted for as noise. Gripped trees do not only change the position of the center of mass, but also the mass of the upper carriage and therefore introduce an additional model error. In a long term view, the mass of the upper carriage could be an additional state variable, being estimated by the pressure of the crane's cylinders.

5 Conclusions

In this article, a measurement model for the correlation between hydraulic pressures in the actuators of each leg and the movement of the upper carriage's center of mass was derived for a portal advancing mechanism. Therefore,

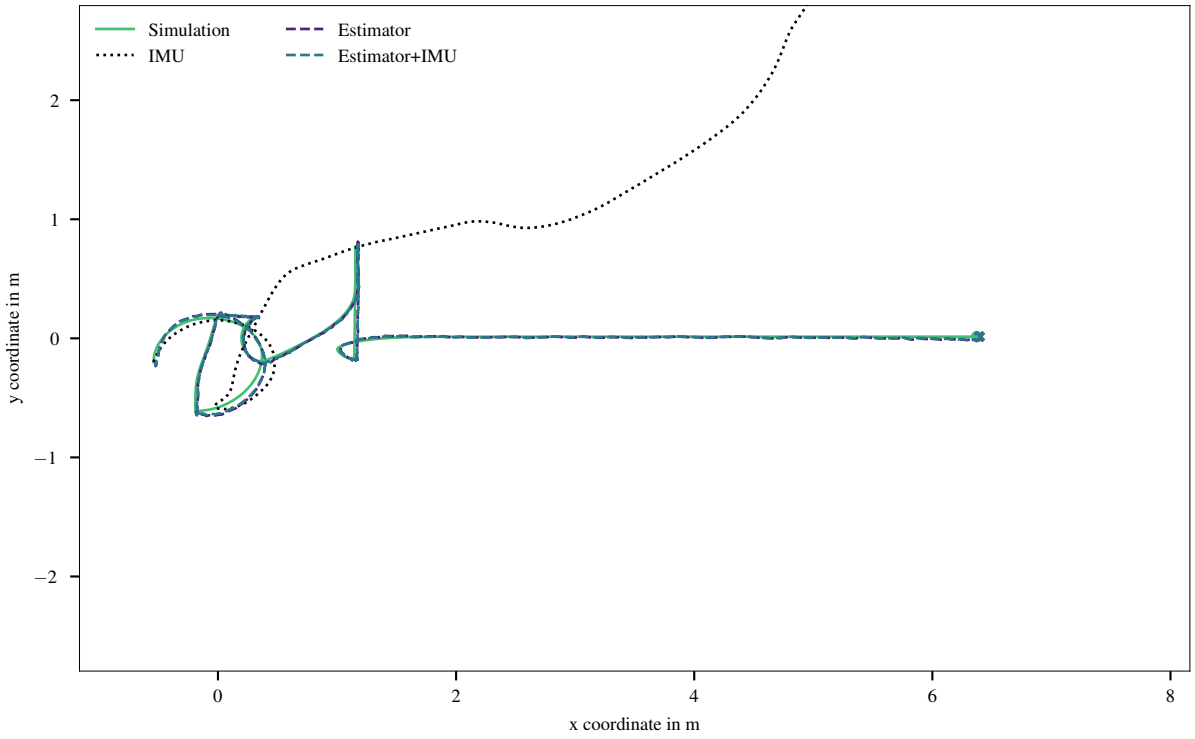

a) Planar movement of the center of mass (x,y)

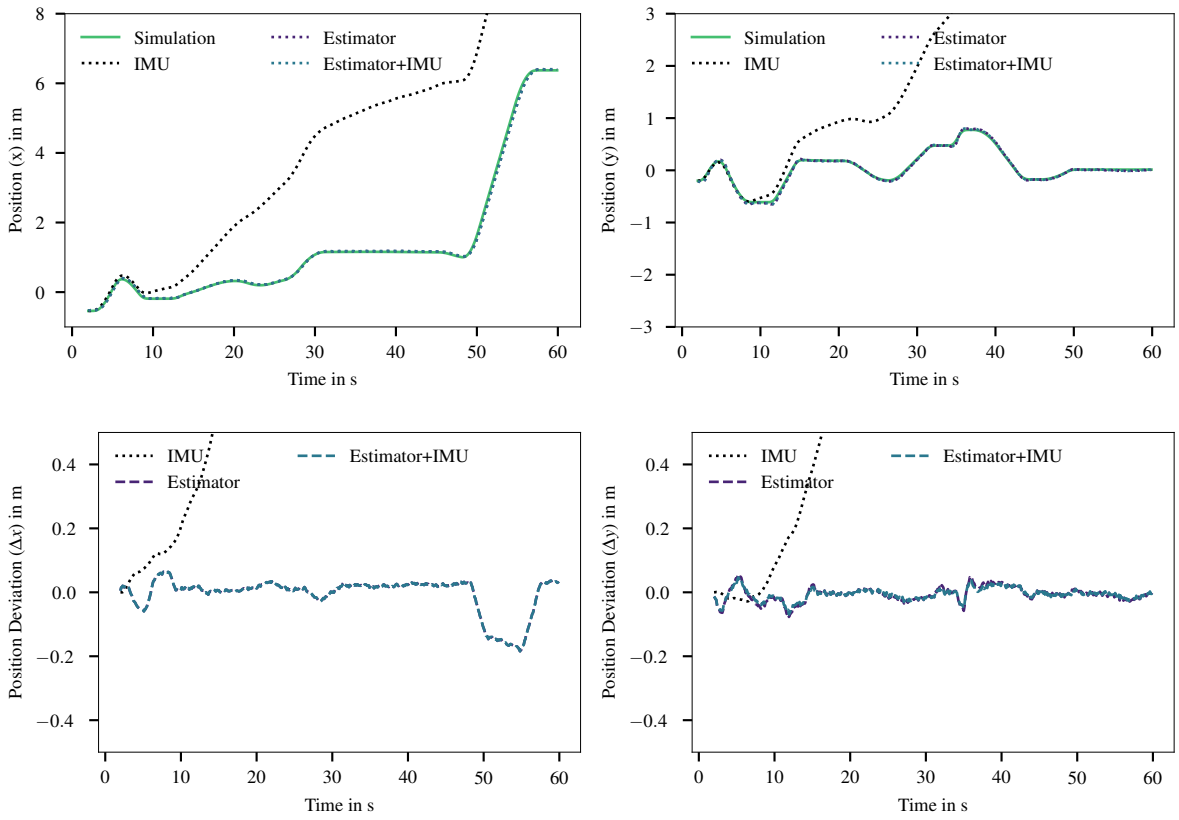

b) Estimated position (x,y) and deviation of the estimated position (Δx,Δy)

Figure 4: IMU-only, estimator and estimator with IMU performance in cycle 5

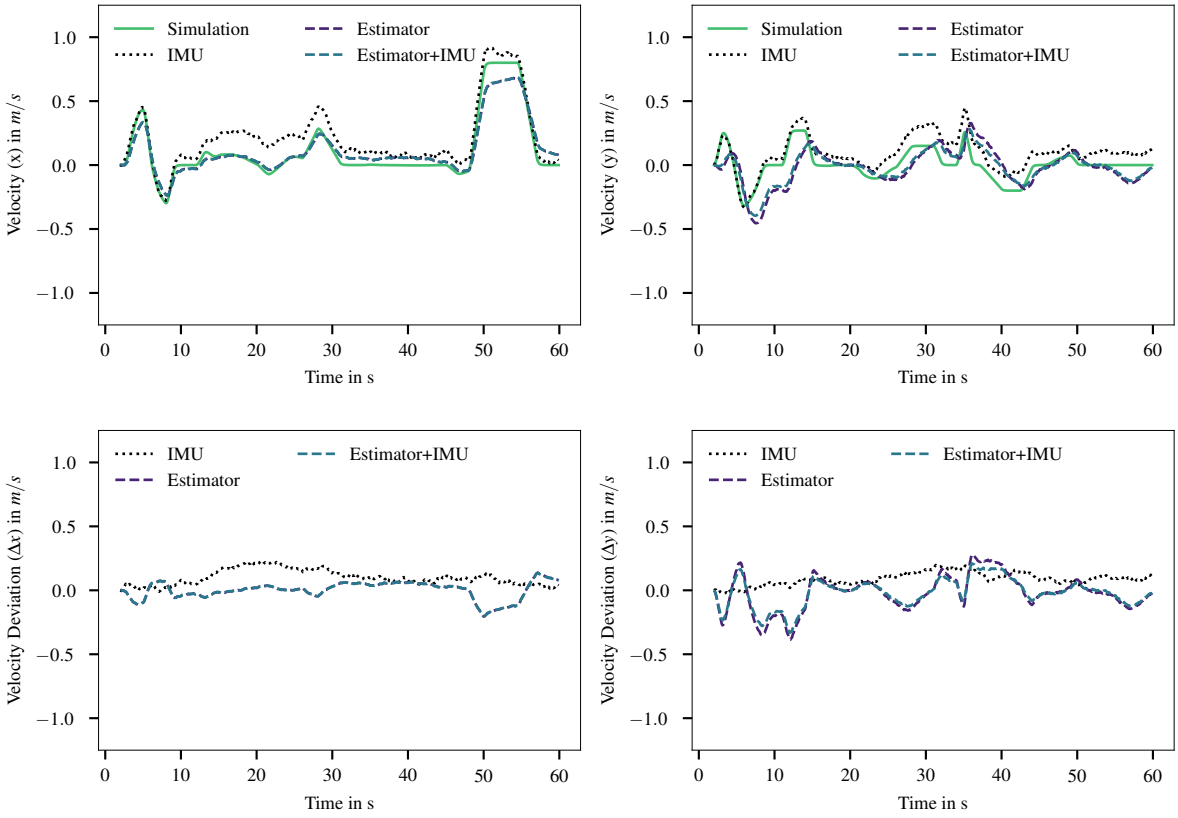

c) Estimated velocity (x,y) and deviation of the estimated velocity (Δx,Δy)

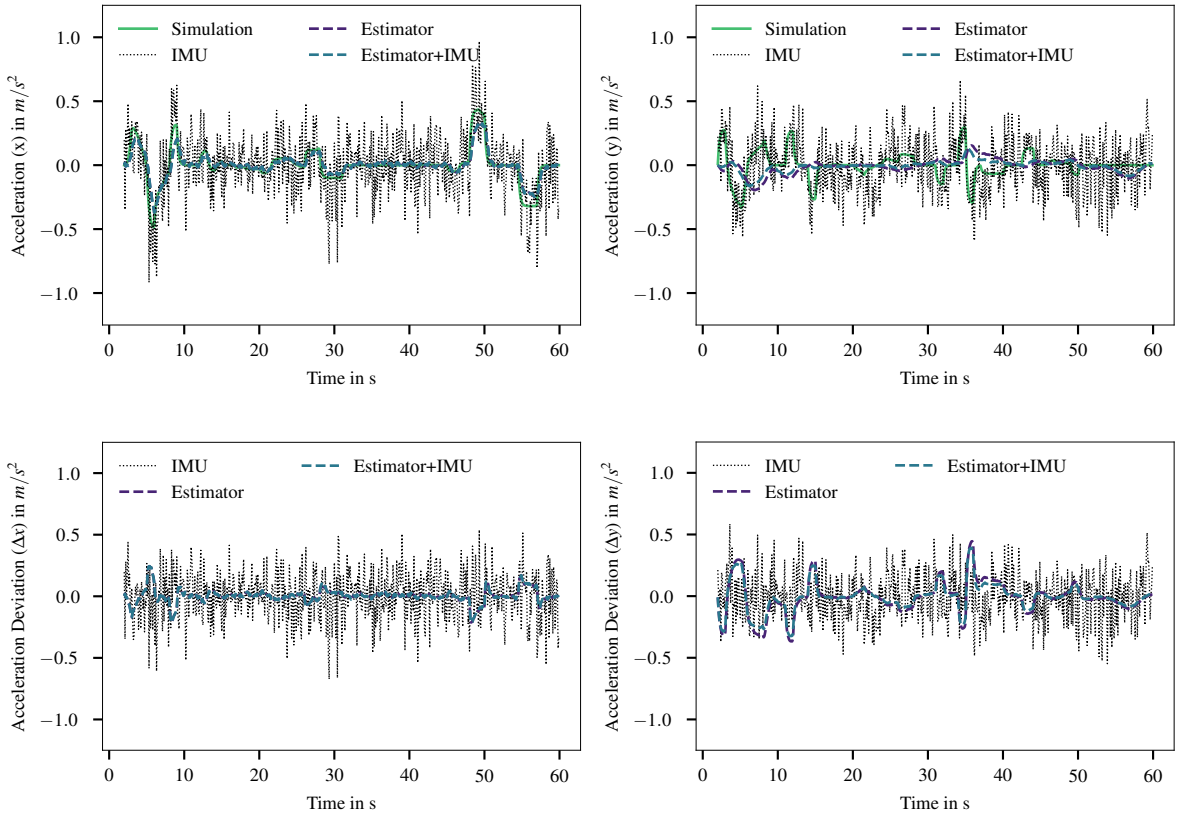

d) Estimated acceleration (x,y) and deviation of the estimated acceleration (Δx,Δy)

Figure 4: IMU-only, estimator and estimator with IMU performance in cycle 5 (cont.)

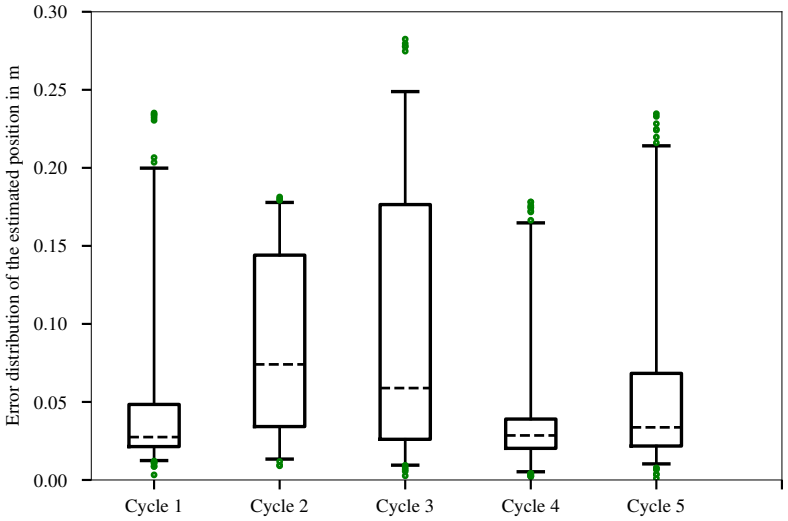

a) Error distribution of the estimated positions, the box extends from the lower to upper quartile with a median line (dashed) and whiskers from 2.5 to 97.5%.

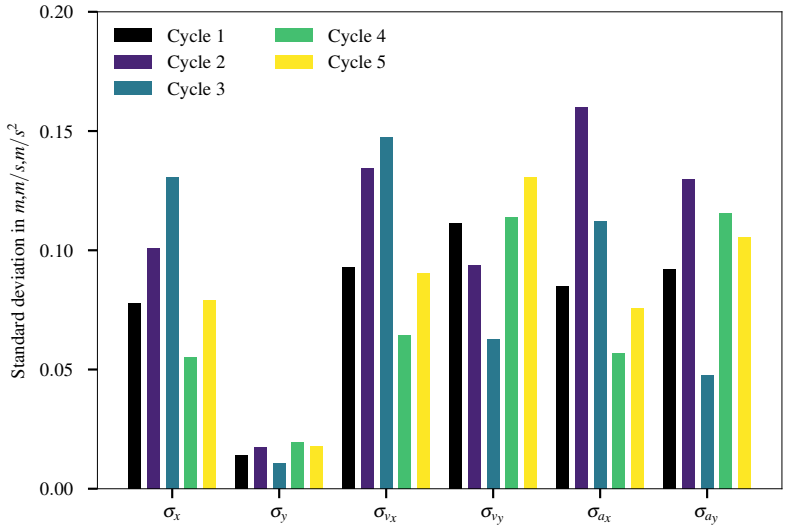

b) State standard deviation

Figure 5: Estimation error and standard deviation of the five monte carlo runs.

a set of additional equations was introduced to the system. With this measurement model and a simple linear movement model, an Extended Kalman Filter was set up to estimate the position of the upper carriage. The used data were generated with a simplified simulation. An IMU system is unable to directly measure the acceleration as the center of mass of the upper carriage is not fixed. Additionally, an IMU system is prone to drift over time and the system's estimation error increased significantly after a short period of time. The proposed estimator was able to provide an accurate position estimation with stationary precision. The implicit velocity and acceleration estimations, however, showed a certain deviation from the true value. It was observed that the integration of additional IMU data into the system does not significantly improve the accuracy of the estimation. In all test cases, a position error of less than 0.3 m was achieved. In future work, the measurement model and the simulation model should be improved in order to get a more realistic representation of the machine. The measurement model can be improved, for example, by considering the distance between the z-axis of the mass of the upper carriage and the rotation axis of the bases. In the simulation model, an additional model for the gripping of a tree could be included.

References

[1] Michael Renner, Sean Sweeney, and Jill Kubit. Green Jobs: Towards Decent Work in a Sustainable, Low-Carbon World (Full report). Report, United Nations Environment Programme (UNEP), 2008.

[2] Edo Jelavic, Pascal Egli, Dominic Jud, and Marco Hutter. Towards Autonomous Robotic Precision Harvesting: Mapping, Localization, Planning and Control for a Legged Tree Harvester. *Field Robotics*, 2021.

[3] J. R. Williamson and W. A. Neilsen. The influence of forest site on rate and extent of soil compaction and profile disturbance of skid trails during ground-based harvesting. *Canadian Journal of Forest Research*, 30:1196–1205, 2000.

[4] Martina Cambi, Giacomo Certini, Francesco Neri, and Enrico Marchi. The impact of heavy traffic on forest soils: A review. *Forest Ecology and Management*, 338:124–138, February 2015.

[5] Marcus Geimer. *Mobile working machines*. SAE International, Warrendale, Pennsylvania (USA), 2020.

[6] Fachagentur Nachwachsende Rohstoffe e.V. Verbundvorhaben: Portalschreitwerk als Fortbewegungsprinzip auf befahrungssensiblen Boeden und zerkluefteten Untergruenden; Teilvorhaben 2: Entwicklung der Steuerungsarchitektur - Akronym: Portalschreitwerk, https://www.fnr.de/index.php?id=11150fkz=2220nr216b, 2021.

[7] Sebastian Beiser and Marcus Geimer. Estimation of Soil Pressures Based on the Pressures in the Hydraulic System for a Legged Forestry Machine. In *Proceedings of the Joint 44th Annual Meeting of Council on Forest Engineering (COFE), the 54th International Symposium on Forest Mechanization (FORMEC) and 2022 IUFRO All-Division 3 Meeting*, pages 174–184, Corvallis, Oregon, USA, October 2022.

[8] Michael Bloesch, Marco Hutter, Mark Hoepflinger, Stefan Leutenegger, Christian Gehring, C. David Remy, and Roland Siegwart. State Estimation for Legged Robots - Consistent Fusion of Leg Kinematics and IMU. *Robotics: Science and Systems VIII*, 2013.

[9] Ola Lindroos, Pedro La Hera, and Carola Häggström. Drivers of Advances in Mechanized Timber Harvesting - a Selective Review of Technological Innovation. *Croatian Journal of Forest Engineering*, 38(2):243–258, 2017.

[10] Thomas Hellström, Pär Lärkeryd, Tomas Nordfjell, and Ola Ringdahl. Autonomous Forest Vehicles: Historic, envisioned, and state-of-the-art. *International Journal of Forest Engineering*, 20(1):31–38, January 2009.

[11] Dominic Jud, Simon Kerscher, Martin Wermelinger, Edo Jelavic, Pascal Egli, Philipp Leemann, Gabriel Hottiger, and Marco Hutter. HEAP - The autonomous walking excavator. *Automation in Construction*, 129, September 2021.

[12] Edo Jelavic, Tun Kapgen, Simon Kerscher, Dominic Jud, and Marco Hutter. Harveri : A Small (Semi-) Autonomous Precision Tree Harvester. In *IEEE International Conference on Robotics and Automation, Innovation in Forestry Robotics: Research and Industry Adoption Workshop*, Philadelphia, PA, USA, May 2022.

[13] Amit Mohanty and Bin Yao. Indirect Adaptive Robust Control of Hydraulic Manipulators With Accurate Parameter Estimates. *IEEE Transactions on Control Systems Technology*, 19(3):567–575, May 2011.

[14] Qiang Li, Ranyang Li, Kaifan Ji, and Wei Dai. Kalman Filter and Its Application. In *2015 8th International Conference on Intelligent Networks and Intelligent Systems (ICINIS)*, pages 74–77, Tianjin, China, November 2015. IEEE.

[15] Christian Knobloch. *Entwicklung und kombinierte Verwendung eines Portalharvesters und eines mobilen Seilkransystems in forstlichen Verfahren zur vollmechanisierten Holzernte auf befahrungssensiblen, ebenen Standorten*. PhD Thesis, Technische Universitaet Dresden, Dresden, Germany, July 2017.

[16] Richard J. Meinhold and Nozer D. Singpurwalla. Understanding the Kalman Filter. *The American Statistician*, 37(2):123–127, May 1983.

A Appendix

$$\mathbf{R}_{model} = \begin{bmatrix} 1.424e11 & 6.243e10 & -3.454e10 & 2.614e10 & 1.346e11 & -1.813e10 \\ 6.243e11 & 4.693e10 & -2.372e10 & -3.238e10 & 5.681e10 & -4.450e09 \\ -3.454e10 & -2.372e10 & 4.120e10 & 1.887e10 & -5.799e10 & -1.128e10 \\ -2.614e10 & -3.238e10 & 1.887e10 & 3.211e10 & -2.395e10 & -7.261e08 \\ 1.346e11 & 5.681e10 & -5.799e10 & -2.395e10 & 1.555e11 & -1.873e09 \\ -1.813e10 & -4.450e09 & -1.128e10 & -7.260e08 & -1.873e09 & 1.341e10 \end{bmatrix} \tag{33}$$